Morphology control of $Ce_{0.9}Gd_{0.1}O_{1.95}$ nanopowder synthesized by sol–gel method using PVP as a surfactant

Youkun Tao, Jing Shao, Jianxin Wang, Wei Guo Wang*

Division of Fuel cell and Energy Technology, Ningbo Institute of Material Technology & Engineering, Chinese Academy of Sciences, 519 Zhuangshi Road, Ningbo, 315201, China

ARTICLE INFO

ABSTRACT

In this work, well-dispersed nanopowder of $Ce_{0.9}Gd_{0.1}O_{1.95}$ (gadolinia doped ceria, GDC) was synthesized by a novel sol–gel thermolysis method using a combination of citrate acid and polyvinylpyrrolidone (PVP). PVP performed as a surfactant and its amount was optimized in terms of GDC powder morphology. The physical and chemical properties of the resultants were characterized by XRD, TG/DTA, FT–IR, SEM, BET and PSA. From the XRD patterns, well-crystalline cubic fluorite structured GDC was obtained after calcining the precursor at 600 °C. The SEM observation showed an average particle size of about 15 nm for the optimal GDC powder and particle size analysis (PSA) gave a narrow distribution of particle size. The sintering experiment showed a good sinterability and a relative density of 94% was achieved at 1300 °C. The dense sample exhibited an ionic conductivity of 0.017 S cm^{-1} at 600 °C in air.

© 2009 Elsevier B.V. All rights reserved.

1. Introduction

Due to high oxide ion conductivity below 800 °C, gadolinia doped ceria ($Ce_{1-x}Gd_xO_{2-\delta}$) has been intensively studied as an attractive electrolyte to substitute stabilized zirconia for intermediate temperature solid oxide fuel cells (IT-SOFCs) [1,2]. The GDC powders have been synthesized by a number of approaches: solid-state reaction [3], freeze-drying [4], acrylamide polymerization [3,5], coprecipitation [3,6], solution combustion or thermal decomposition [7–10], hydro-thermal [11], etc. Nanocrystalline GDC has been achieved by some of the methods mentioned above; however, the reduction of agglomeration is still a common difficulty. It is well known that in soft chemical synthesis, surfactant addition has an important effect on the solution and microstructure of the resultant. Aiming at obtaining nanopowders with low agglomerations, some attempts had been made by adding special polymers, i.e. polyvinyl alcohol [10,12], to the sol–gel synthesis of $LiMn_2O_4$ or GDC.

In this investigation, a novel method was developed adopting the advantages of sol–gel process and surfactants: an appropriate surfactant (PVP) was introduced into the citrate–metal ion complex to achieve well-dispersed, homogeneous GDC nanopowder. PVP performs not only as a fuel, but also impacts the gelation process and the aggregation of particles during the gel thermolysis due to its long chain structure. The effect of different surfactant amounts on the morphology of the resultant powders was investigated. The precursor pyrolysis and phase formation as well as the ionic conductivity of the sintered bulk were studied.

2. Experimental

GdO_2 (99.99% purity), $Ce(NO_3)_3 \cdot 6H_2O$ (99.99% purity), HNO_3 (65%) and citric acid (99% purity) were provided by Sinopharm Chemical Reagent Co., Ltd., (China) as the starting materials used in the synthesis of $Ce_{0.9}Gd_{0.1}O_{1.95}$. According to the formula $Ce_{0.9}Gd_{0.1}O_{1.95}$, stoichiometric amounts of GdO_2 were dissolved in nitric acid and $Ce(NO_3)_3 \cdot 6H_2O$ was added subsequently to obtain a mixed nitrate aqueous solution. A definite amount of citric acid (CA) with the ratio to overall metal ions of 1.5:1 was added to the solution. Different amounts of PVP were then added as a surfactant denoted as S1 (2×10^{-3} g ml^{-1}), S2 (4×10^{-3} g ml^{-1}), S3 (8×10^{-3} g ml^{-1}), and S4 (1.2×10^{-2} g ml^{-1}), respectively. The precursor solution was heated using water bath at a temperature of 75 °C and stirred continuously for several hours to evaporate the water. The resulting transparent gel-like precursors were obtained, and then dried at 110 °C for 12 h and 250 °C for 5 h. Finally, the obtained yellow ash was heat-treated in a muffle furnace at different temperatures.

TG/DTA analysis was carried out with a heating rate of 5 °C min^{-1} in the air. Fourier transform infrared spectroscopies (FT–IR) of the precursors were measured by the KBr pellet method. The precursors were dried at 110 °C, 250 °C for 12 h and calcined at 600 °C for 2 h, respectively. The resulting powder undergone calcining in stagnant air was investigated by X-ray diffraction (XRD) on the phase evolution. XRD data were collected using Bruker D8 Advance with Cu Kα radiation at a step of 0.02° s^{-1} in the range of 2θ from 20° to 80°. After grinding for a few minutes with a mortar, the synthesized powders were characterized on morphology using a Hitachi S-4800 scanning electron microscopy (SEM). The BET specific surface area was measured using nitrogen adsorption–desorption at 77 K. Further information of powder sizes was obtained using a laser diffraction particle size analyzer (Malvern Nano-ZS).

The resultant GDC powders were fabricated into foils by tape casting followed by sintering at various temperatures. The densities of the sintered samples were measured by Archimedes Principle. Platinum electrodes were prepared using platinum paste both sides of the sample sintered at 1450 °C. The impedance was measured using a frequency response analyzer (Soltron 1260) over a frequency range from 0.1 Hz to 2 MHz at 550–750 °C in air. For comparison, the impedance of YSZ dense

sample after 1400 °C sintering was measured in the same temperature range. The ionic conductivity, σ, was derived from the impedance data and the activation energy (E_a) of the conductivity for GDC was determined by the Arrhenius law: $\sigma T = \sigma_o \exp(-E_a/kT)$, where σ_o is the pre-exponential factor and k is the Boltzmann constant.

3. Results and discussion

In order to study the chelating and pyrolysis processes, the precursors made from the solution with S2 addition were analyzed by the TG/DTA and FT–IR measurements. Fig. 1 shows the TG/DTA curves obtained at a heating rate of 5 °C min^{-1} in air from room temperature to 600 °C for the GDC precursors. The weight loss below 170 °C is due to the dehydration of the precursors and the exothermal peak at 170 °C on the DTA curve is because of the nitrates decomposition which also lead to a weight loss on TG curve and large volume of exhausts observed in experiments. The sharp and strong exothermic peak at 312 °C may be due to the oxidation of the chelate complex along with formation of metal oxides and the steep weight loss curve at this stage may be related to the burn-out of the residual organic compounds. There is an endothermic peak at about 552 °C which may be due to the formation of the main phase. At temperatures above 350 °C, no significant weight loss on TG curve was observed.

Fig. 2 shows the FT–IR spectra for the GDC precursors after pyrolysis or calcinations. In the spectrum of the precursors after drying, absorption band characteristics of nitrate ions ($\sim$1380 cm^{-1} and 840 cm^{-1}) are clearly observed. The symmetric ($\sim$1080 cm^{-1}) and asymmetric ($\sim$1040 cm^{-1}) C–O stretching can be seen in Fig. 2 as well as asymmetric stretching vibrations of COO^{-} at $\sim$1590 cm^{-1} and the symmetric COO^{-} stretching at $\sim$1420 cm^{-1}. The carbonyl absorptions are shifted to lower frequencies with respect to pure citric acid and similar phenomena were reported in other metal–citrate complexes by Liu et al. [13] and Matzapetakis et al. [14]. This indicates a change in the vibrational status of the citrate anion upon coordination to the metal ions. In the spectrum of the precursor subjected to heat treatment at 250 °C, the NO$_3^-$ vibration ($\sim$1380 cm^{-1}) is still observed, but the intensity of the peak decreases greatly. The broad absorption band in the 400–650 cm^{-1} interval could be ascribed to metal–oxygen band. Therefore the FT–IR analysis result is in good agreement with TG/DTA results for the thermal decomposition process of the precursors as discussed above.

The XRD patterns for the resultant GDC powders after calcinations at various temperatures are shown in Fig. 3. It can be seen that single perovskite phase is formed after heat treatment at 600 °C for 2 h and the XRD patterns become sharper with increasing calcining temperature indicating the gradual growth of the crystallite size of the GDC powder. All samples show main reflections of cubic fluorite structure of GDC corresponding to (1 1 1), (2 0 0), (2 2 0), (3 1 1),
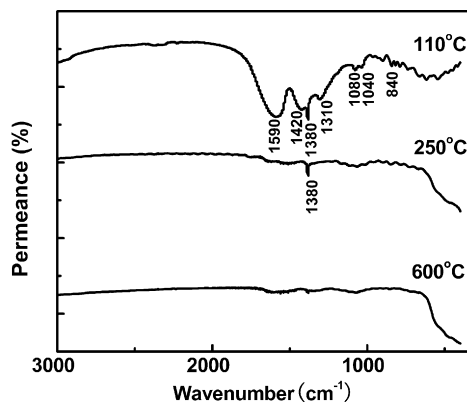

Fig. 2. FT–IR spectra of the precursors before and after various heat treatments.

(2 2 2) and (4 0 0) planes which are in good agreement with PDF: 01–075–0161. The elemental composition analysis of the resulted GDC powders was determined by XRF (ZSX Primu II) and the result (CeO$_2$ 90%, Gd$_2$O$_3$ 9.88%) was fairly consistent with the expected composition.

SEM morphologies of the GDC powders are presented in Fig. 4. The samples were derived from different surfactant conditions and heat-treated at 600 °C for 2 h. It is observed that sample S1 (Fig. 4a) has a mean powder size of approximately 60 nm that is the largest size among all powders. Also, the particles tend to agglomerate rather than homogeneously distributed. When the surfactant amount increases, the powder morphology varies significantly. For GDC derived from solutions with S2 added, the powder is highly homogeneous and well-dispersed as shown in Fig. 4b. The powders are in spherical shapes with a diameter of about 15 nm, which is the smallest size of all powders. With the addition of S3 (Fig. 4c) the powder size increases to 30–40 nm while the powder with S4 (Fig. 4d) has a larger size and slight agglomeration. This indicates that the morphology of GDC powder could be carefully tailored by controlling the surfactant in the synthesis process. It is shown that the optimized shape of the GDC can be achieved by adding surfactant S2.

The effect of the surfactant may be explained by the polymerizations and steric interactions [15]. All the reactants were chelated and mixed uniformly in solution at atomic or molecular level. The surfactant molecules were absorbed on the colloidal particles and polymerized with the carboxyl of CA. The long chain structure tended to extend the distance of colloids and avoid interpenetration, and further impacted the gelation process as well as the gel thermolysis. Considering the effect varied with the amount of surfactant addition, the particle size and the aggregation of particles
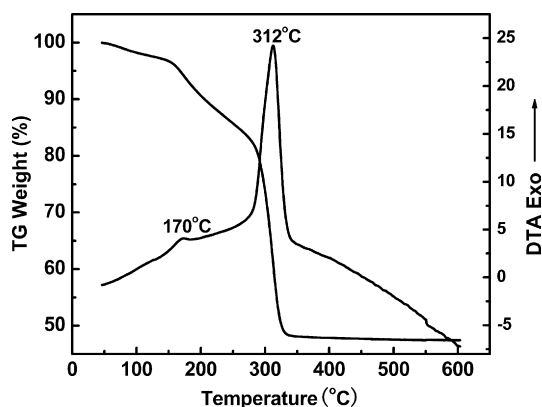

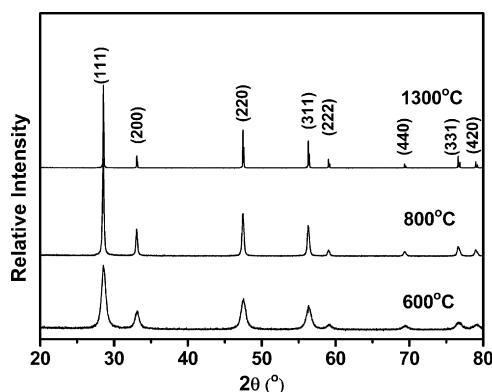Fig. 1. TG/DTA plots for the as-synthesized GDC precursors.

Fig. 3. XRD patterns of the GDC powder calcined at different temperatures.
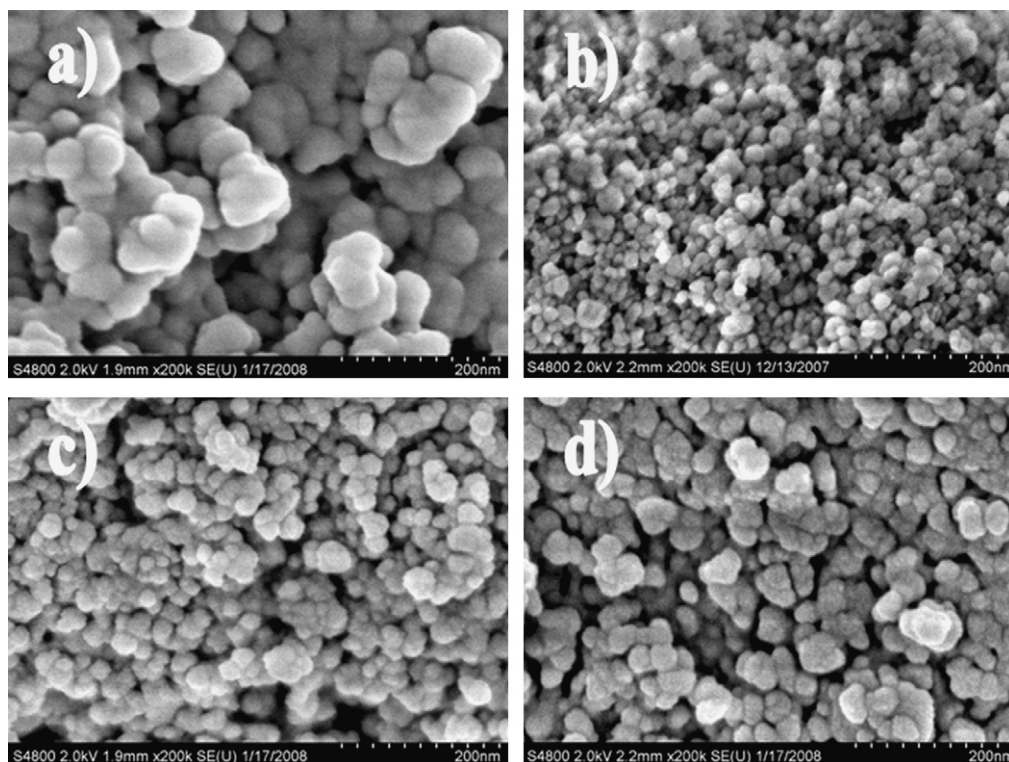
Fig. 4. SEM photographs of the GDC powders derived from different surfactants: (a) S1, (b) S2, (c) S3 and (d) S4.

can be carefully controlled. The particle size grew after heat treatments but retained high uniformity.

The corresponding BET specific area was measured to be $18.8\,m^2\,g^{-1}$ and, assuming all particles are spherical, the average particle size (d_{BET}) can be calculated using

$$d_{BET} = \frac{6}{(\rho S_v)} \tag{1}$$

where ρ is the materials density and S_v is the surface area of the sample, and the calculated d_{BET} for the powder is 44 nm. The particle size analysis (PSA) was carried out by the laser diffraction particle size analyzer; the statistics data reveal a mono-modal particle size distribution (Fig. 5), 75% of the powders are within the size range of 80–90 nm. In literature reports [10], GDC particle size from PSA was much larger than that from TEM, XRD or BET, which indicated large numbers of agglomerations. The GDC particle size from PSA in this work is close to that from BET and SEM and the particle size distribution is quite narrow, which indicates low agglomer-
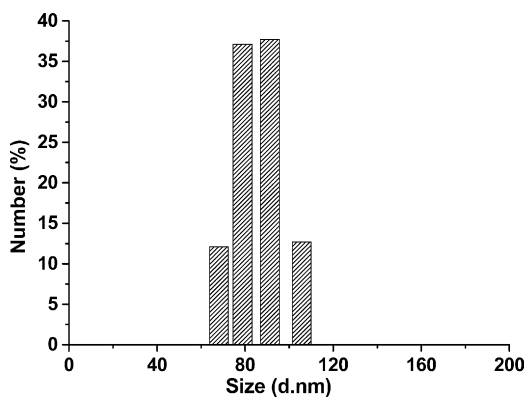
ation and well-dispersed powders. The different average particle sizes obtained from SEM, BET and PSA were probably related to the powder sample property or the characterization method itself. Although no identical particle size can be obtained by the above-mentioned measurements, we believe the particles are less than 100 nm, and with narrow distribution and low aggregation, which is of more concern. Moreover, the advantage of this unique synthesis method is reliable to scale up. Each time 100 g of the above GDC powders were yield in the experiment.

The green tapes made from the powders by tape casting were sintered in stagnant air at various temperatures. The relative densities of the sintered samples are plotted as a function of the sintering temperature as shown in Fig. 6. After sintering at 1200 °C, the relative density reaches 90% indicating the sintering behavior already occurred. The sample sintered at 1300 °C and 1450 °C obtain a relative density of 94% and 98.2%, respectively. The values are higher than those of GDC powders prepared by solid-state reaction, freeze-
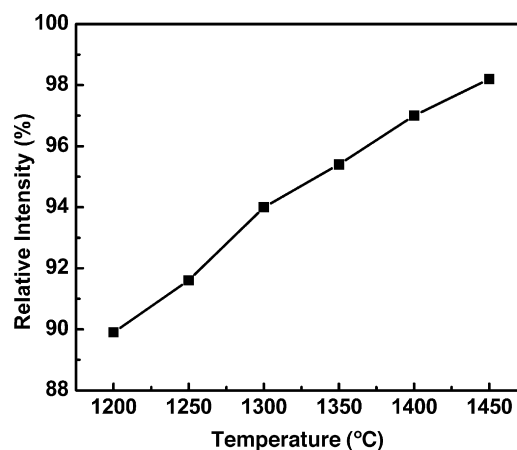

Fig. 5. Mono-modal particle size distribution of the GDC powders synthesized with S2.

Fig. 6. Relative densities of the GDC samples sintered at different temperatures.
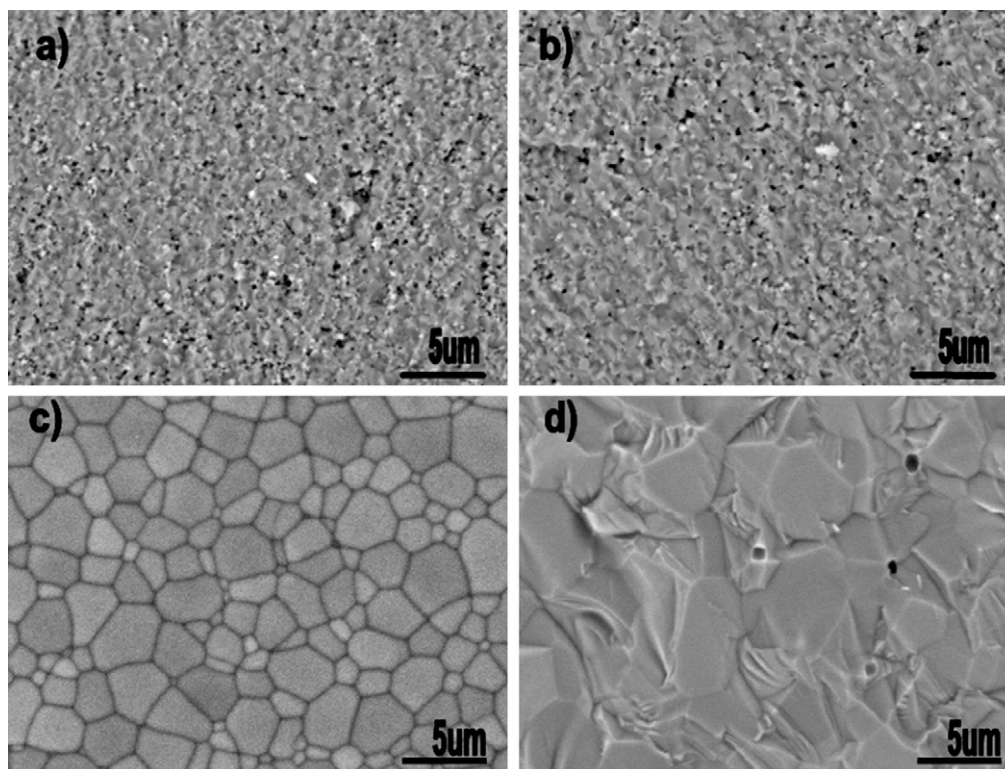
Fig. 7. SEM microstructure of the GDC sintered at various temperatures: cross-section view for (a) 1200 °C, (b) 1300 °C, (d) 1450 °C and surface view for (c) 1450 °C.

drying (∼95% for 1600 °C) [16] and mechanochemical synthesis (∼98% for 1550 °C) [17], and similar to those from coprecipitation, acrylamide polymerization sol–gel (∼95% for 1450 °C) [3] or gel-casting process (∼96% for 1450 °C) [18]. This indicates the high sinterability of the well-dispersed GDC nanopowders.

The SEM micrographs in Fig. 7 demonstrate the densification of GDC ceramics at around 1300 °C, and are in good agreement with the relative density results in Fig. 6. A decrease in the porosity is observed by SEM with the rising sintering temperature. After 6 h sintering at 1450 °C, the sample appears almost completely dense (Fig. 7d), which confirmed the high relative density measured. The mean crystal grain size grew from about 1 μm for 1300 °C to about 5 μm for 1450 °C. Grain boundaries are also found poorly defined between particles, which indicate a material interdiffusion among the grains and a reduction in the extent of grain boundaries.
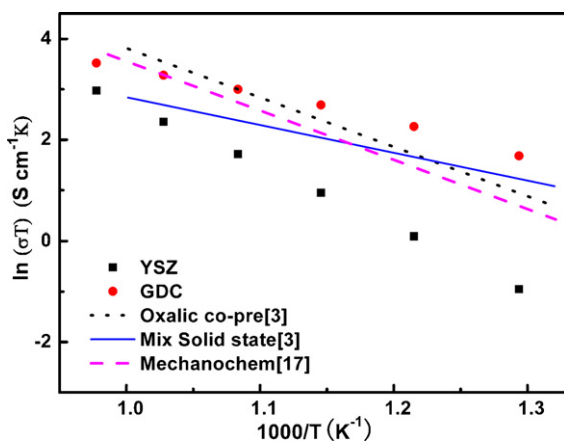
The impedance spectra were measured from 500 °C to 750 °C for the dense pellets of GDC and YSZ. The Arrhenius plots of the conductivity for the two samples are shown in Fig. 8. The GDC sample shows better conductivities than YSZ and the conductivity at 600 °C is 0.017 S cm^{-1} for GDC while 0.003 S cm^{-1} for YSZ. The dense GDC ceramic exhibits an ionic conductivity similar to those reported in the literature [3,17]. The activation energy is 0.49 eV for the GDC ceramic in this work, which is a little smaller than the reported values.

4. Conclusions

Nanocrystalline $Ce_{0.9}Gd_{0.1}O_{1.95}$ has been successfully synthesized by an improved sol–gel method. It is found that the amount of the surfactant (PVP) imposes a significant effect on the powder morphology and the powder shape is optimized. The optimal surfactant addition S2 results the well-dispersed, homogeneous GDC with powder sizes of 10–15 nm. The single fluorite structure forms completely at a temperature of 600 °C. The sintered $Ce_{0.9}Gd_{0.1}O_{1.95}$ sample exhibits an ionic conductivity of 0.017 S cm^{-1} in air at 600 °C, which can be, used as an electrolyte material for IT-SOFCs. The combination of citrate and PVP is proved to be an effective method in synthesis of low aggregation GDC nanopowder.

Fig. 8. Arrhenius plot of ionic conductivity of sintered GDC (synthesized in this work) and YSZ ceramics.

References

[1] M. Mogensen, N.M. Sammes, G.A. Tompsett, Solid State Ionics 129 (2000) 63–94.

[2] R.M. Ormerod, Chem. Soc. Rev. 32 (2003) 17–28.

[3] A. Sin, Y. Dubitsky, A. Zaopo, A.S. Aricò, L. Gullo, D. La Rosa, S. Siracusano, V. Antonucci, C. Oliva, O. Ballabio, Solid State Ionics 175 (2004) 361–366.

[4] D. Pérez-Coll, P. Núñez, J.R. Frade, J.C.C. Abrantes, Electrochim. Acta 48 (2003) 1551–1557.

[5] A. Tarancón, G. Dezanneau, J. Arbiol, F. Peiró, J.R. Morante, J. Power Sources 118 (2003) 256–264.

[6] S. Zha, C. Xia, G. Meng, J. Power Sources 115 (2003) 44–48.

[7] T. Mahata, G. Das, R.K. Mishra, B.P. Sharma, J. Alloys Compd. 391 (2005) 129–135.

[8] R.K. Lenka, T. Mahata, P.K. Sinha, A.K. Tyagi, J. Alloys Compd. 466 (2008) 326–329.

[9] R.D. Purohit, B.P. Sharma, K.T. Pillai, A.K. Tyagi, Mater. Res. Bull. 36 (2001) 2711–2721.

[10] D.H. Prasad, J.-W. Son, B.-K. Kim, H.-W. Lee, J.-H. Lee, J. Eur. Ceram. Soc. 28 (2008) 3107–3112.

[11] S. Dikmen, P. Shuk, M. Greenblatt, H. Gocmez, Solid State Sci. 4 (2002) 585–590.

[12] A. Subramania, N. Angayarkanni, T. Vasudevan, Mater. Chem. Phys. 102 (2007) 19–23.

[13] S. Liu, K. Li, R. Hughes, Mater. Res. Bull. 39 (2004) 119–133.

[14] M. Matzapetakis, C.P. Raptopoulou, A. Tsohos, V. Papaefthymiou, N. Moon, A. Salifoglou, J. Am. Chem. Soc. 120 (1998) 13266–13267.

[15] A.C. Pierre, Introduction to Sol–Gel Processing, 1st ed., Kluwer Academic Publishers, London, 1998, pp. 155–158.

[16] D. Pérez-Coll, J.C. Ruiz-Morales, D. Marrero-López, P. Núñez, J.R. Frade, J. Alloys Compd. 467 (2009) 533–538.

[17] K. Maca, J. Cihlar, K. Castkova, O. Zmeskal, H. Hadraba, J. Eur. Ceram. Soc. 27 (2007) 4345–4348.

[18] J.-G. Cheng, S.-W. Zha, J. Huang, X.-Q. Liu, G.-Y. Meng, Mater. Chem. Phys. 78 (2003) 791–795.